Kinetics of Nested Inorganic Fullerene-like Nanoparticle Formation

Y. Feldman, V. Lyakhovitskaya, and R. Tenne*

Contribution from the Department of Materials and Interfaces, Weizmann Institute of Science, Rehovot 76100, Israel

Received September 11, 1997

Abstract: Recently, a model for the growth mechanism of inorganic fullerene-like (IF) nanoparticles of MS_2 (M = Mo, W) from the respective oxides was presented (Feldman, Y.; Frey, G. L.; Homyonfer, M.; Lyakhovitskaya, V.; Margulis, L.; Cohen, H.; Hodes, G.; Hutchison, J. L.; Tenne, R. *J. Am. Chem. Soc.* **1996**, *118*, 5362). According to this model, sulfidization of oxide particles of <150 nm leads to the formation of a sulfide encapsulate with oxide core, which is progressively converted into a hollow IF nanoparticle. Using transmission electron microscopy, the sulfidization of a group of oxide nanoparticles is demonstrated step by step. This study provides direct evidence for the quasi spiral growth of the sulfide layers into the oxide nanoparticle core. However, the mechanism for the formation of the first closed sulfide layer which engulfs the oxide encapsulate remained a puzzle thus far. The analysis of the kinetics of simultaneous reduction and sulfidization of WO_3 powders suggests the occurrence of a unique *driving force* for the fast growth of the first curved sulfide layer (001) around an oxide nanoparticle. According to the present model, a *synergy between the reduction and sulfidization* processes which occurs in a very narrow window of parameters leads to the formation of the first one or two closed sulfide layers. The present study is not limited to the sulfides. The formation of IF−WSe_2 (Tsirlina, T.; Feldman, Y.; Homyonfer, M.; Sloan, J.; Hutchison, J. L.; Tenne, R. *Fullerene Sci. Technol.* **1998**, *6*, 157) is found to be consistent with the same kind of model.

1. Introduction

Real crystals have many random point defects that lead to a curvature of the crystallographic planes in their close proximity. However, in some materials, like mineral structures, such as clino-asbestos, cylindrite, and halloysite, long-range order of curved atomic layers exists.[3,4] Bursill developed the idea of a spiral lattice as a new type of crystallography, based on the Archimedian spiral.[5]

The most outstanding example of sphere-like curved atomic structure is found in the case of the fullerenes.[6] Nested fullerenes (onion-like structures)[7] and nanotubes[8] further extend the concept of spherical symmetry in molecules up to the size of nanoparticles (>3 nm) and beyond. The discovery of fullerenes stimulated the search for similar structures in other layered compounds. Hexagonal boron nitride, having a layer structure similar to that of graphite, shows a tendency toward curling and forming concentric shells with onion-like structures.[9,10] Earlier, layered compounds with more complicated structure, such as MS_2 (M = Mo, W), were shown to form onion-like nanoparticles (inorganic fullerene-like, IF) and nanotubes.[11−13]

A general mechanism for fullerenes' formation has been proposed[14,15] in which the small graphitic sheets bend in an attempt to eliminate the large number of highly energetic dangling bonds present at the edges of the growing nanostructure. The experimental techniques for the production of carbon fullerene molecules include laser vaporization,[14,16] arc discharge,[17−20] and electron irradiation.[21−26]

Boron nitride[9] and MoS_2[27] onion-like nanoparticles were obtained under intense irradiation in transmission electron microscope (TEM). MoS_2 onion-like nanoparticles were obtained also from amorphous MoS_3 by short electrical pulses from the tip of a scanning tunneling microscope.[28] Most likely, the driving force here involves energy minimization of the dangling

(1) Feldman, Y.; Frey, G. L.; Homyonfer, M.; Lyakhovitskaya, V.; Margulis, L.; Cohen, H.; Hodes, G.; Hutchison, J. L.; Tenne, R. *J. Am. Chem. Soc.* **1996**, *118*, 5362.
(2) Tsirlina, T.; Feldman, Y.; Homyonfer, M.; Sloan, J.; Hutchison, J. L.; Tenne, R. *Fullerene Sci. Technol.* **1998**, *6*, 157.
(3) Whittaker, E. J. W. *Acta Crystallogr.* **1955**, 571.
(4) Yada, K. *Acta Crystallogr. A* **1971**, *27*, 659.
(5) Bursill, L. A.*Int. J. Modern Phys. B* **1990**, *4*, 2197.
(6) Kroto, H. W.; Heath, J. R.; O'Brien, S. C.; Curl, R. F.; Smalley, R. E. *Nature* **1985**, *318*, 162.
(7) Iijima, S. *J. Cryst. Growth* **1980**, *50*, 675.
(8) Iijima, S. *Nature* **1991**, *354*, 56.
(9) Banhart, F.; Zwanger, M.; Muhr, H.-J. *Chem. Phys. Lett.* **1994**, *231*, 98.
(10) Boulager, L.; Andriot, B.; Cauchetier, M.; Willaime, F. *Chem. Phys. Lett.* **1995**, *234*, 227.
(11) Tenne, R.; Margulis, L.; Genut, M.; Hodes, G. *Nature* **1992**, *360*, 444.
(12) Margulis, L.; Salitra, G.; Tenne, R.; Talianker, M. *Nature* **1993**, *365*, 113.
(13) Feldman, Y.; Wasserman, E.; Srolovitz, D. J.; Tenne, R. *Science* **1995**, *267*, 222.
(14) Zhang Q. L.; et al. *J. Phys. Chem.* **1986**, *90*, 525.
(15) Goroff, Nancy S. *Acc. Chem. Res.* **1996**, *29*, 77.
(16) Kroto, H. W. *Nature* **1987,** *329*, 529.
(17) Krätschmer, W. A.; Lamb, L. D.; Fostiropoulos, K.; Huffman, D. R. *Nature* **1990**, *347*, 354.
(18) Guo, T.; Jin, C.; Smalley, R. E. *J. Phys. Chem.* **1991**, *95*, 4948.
(19) Saito, Y.; Yoshikawa, T.; Inagaki, M.; Tomita, M.; Hayashi, T. *Chem. Phys. Lett.* **1993**, *204*, 277.
(20) Jiao, J.; Zhou, D.; Seraphin, S. *ICEM 13*, Paris, July 17−22, 1994.
(21) Ugarte, D. *Nature* **1992**, *359*, 707; *Eur. Phys. Lett.* **1993**, *22*, 45; *Chem. Phys. Lett.* **1993**, *207*, 473; *MRS Bull.* November 1994.
(22) Zhang, Y.; Wei, Y.; Jian, L.; Zhan, K.; Lin, S. *Phys. Rev. Lett.* **1995**, *74* (14), 2717.
(23) Zwanger M. S.; Banhart, F. *Philos. Mag. B* **1995**, *72* (1), 149.
(24) Burden, A. P.; Hutchison, J. L. *J. Cryst. Growth* **1996**, *158*, 185.
(25) Zwanger, M. S.; Banhart, F.; Seeger, A. *J. Cryst. Growth* **1996**, *163*, 445.
(26) Fuller, Th.; Banhart, F. *Chem. Phys. Lett.*
(27) Jose-Yacaman, M.; Lorez, H.; Santiago, P.; Galvan, D. H.; Garzon, I. L.; Reyes, A. *Appl. Phys. Lett.* **1996**, *69* (8), 1065.

S0002-7863(97)03205-8 CCC: $15.00
Published on Web 04/18/1998

bonds which are formed during crystallization of the amorphous nuclei.

Curved layers can be formed also by a chemical reaction on a curved template. Bursill shows high-resolution TEM (HREM) images of nickel sulfide core structures surrounded by tungsten sulfide sheets.[5] Sanders showed MoS_2 spherical nanoparticles,[29] which were observed in hydrodesulfurization catalysts of some oxides. HREM was used for investigating the influence of curvature on electron diffraction of the nanoparticles. An almost pure nested fullerene-like (IF) phase (hollow onion-like nanoparticles) and nanotubes of MoS_2 were synthesized by a gas-phase reaction (GPR).[13] Another setup for the synthesis of about 1 g/day of IF−WS_2 by solid−gas reaction (SGR) was realized.[1] In both reactions, oxide particles serve as precursors for the IF phase formation.

Recently, a model for IF−MS_2 formation from oxide nanoparticles in H_2S atmosphere was suggested.[1] According to this model, under certain conditions, one or two layers of molybdenum/tungsten disulfide encage the surface of the corresponding oxide nanoparticles in a very fast process (<5 s). Subsequently, the reduced oxide core of the nanoparticle is progressively converted into sulfide nanoparticle with an empty core. This process may take 15−120 min depending on the experimental parameters.

To unravel the mechanism of the IF formation, the kinetics of the oxide reduction/sulfidization was studied. A detailed description of the synthesis of IF has been reported previously[1,13] and will be repeated only briefly here. Both GPR and SGR are used for IF synthesis by sulfidization of oxide powder in reducing atmosphere (mixture of H_2S and forming gas, typically (95% N_2/5% H_2)) at elevated temperatures (∼800 °C). Since molybdenum oxide is volatile above 700 °C, the GPR was adopted for synthesis of IF−MoS_2. Consequently, the size of IF−MoS_2 is determined primarily by the reaction parameters. In this case the shape and size of the precursor (molybdenum oxide) particles can be controlled by varying the reaction conditions. Tungsten oxide is not volatile at least until 1000 °C, and hence, SGR was opted for the synthesis of IF−WS_2. Therefore the size of IF−WS_2 depends only on the size of the incipient oxide nanoparticles which must be less than 200 nm. For this reason, the tungsten oxide into IF−WS_2 conversion was preferred for the present kinetic study.

While previous studies helped to elucidate the growth mechanism of the IF particle after the first few layers have been formed, the great puzzle which remains to be understood is the formation of the first one or two closed sulfide layers on top of the oxide nanoparticle. This closed sulfide layer serves as a template for the furthering of IF growth. Its formation is counterintuitive to thermodynamic arguments, since the elastic energy of bending must be accounted for. To address this central issue, the kinetics of the IF synthesis from the respective oxide nanoparticles and the chalcogen gas are further studied. A kinetic model which takes into account the synergy between the formation of shear planes within the oxide nanoparticle and the surface sulfidization reaction is described. The predictive power of this model is tested by using a number of test cases which are described in the text.

2. Experimental Section

The procedures for the synthesis of the IF particles are similar to the ones described in earlier publications.[1,13]

For the synthesis of IF−MoS_2,[13] a portion of 30 mg of MoO_3 powder (>99% pure) is heated (>800 °C) and sublimes and effuses out of a nozzle where it crosses a stream of H_2S gas mixed with a forming gas (95% N_2/5% H_2). It takes some 3−5 min for the entire load of MoO_3 to sublime. The reaction products are collected on a quartz substrate, which is positioned 3 cm away from the crossing point of the two gas streams and is maintained at the same temperature (>800 °C).

Since WO_3 is not volatile at these temperatures, the solid (WO_3)−gas (H_2S + H_2) reaction was preferred, in this case.[1] The starting material for the synthesis of IF−WS_2 is a WO_3 powder (>99% pure), with particle sizes smaller than ca. 150 nm. To avoid agglomeration and fusion of the heated nanoparticles, the powder was carefully dispersed on the entire floor of the reactor boat, resulting in a complete exposure of the nanoparticle surface to the reacting gas. 2H−WS_2 platelets were predominantly obtained under the following experimental conditions: packing of the powder was too compact; oxide particles with sizes above 0.2 μm were used; reaction temperature exceeded 900 °C.

Samples were cooled to room temperature before removing them from the reactor. They were immediately transferred to a vacuum desiccator and kept there until shortly before the analysis. A sample from the reaction product was collected on a Cu grid covered with amorphous carbon film and examined by CM12 (Philips) TEM. For the XRD experiments, a Rigaku Rotaflex RU-200B powder diffractometer with a Cu anode was used.

For the HREM analysis, a JEOL 3010 microscope equipped with 300-keV beam was used. A sample of molybdenum oxide was first sulfidized in the GPR for 5 min.[13] A group of the partially sulfidized nanoparticles was dispersed on a gold grid with SiO support which can withstand the severe conditions in the reactor chamber was used. Moreover, this grid has ABC marks which help to locate the same specimen again and again. After the first HREM examination, the same grid was inserted back into the reactor and the sulfidization reaction was repeated for another 10 min. Subsequently, the grid was removed from the reactor and reexamined by the HREM.

3. Results

3a. Direct Evidence for the IF Growth Mechanism. In previous works,[1,13] IF formation from oxide nanoparticles was followed by retracting a portion of the powder from the reactor at different times and analyzing the powder using various techniques. To get a more firm picture of the IF growth model, it would be desirable to follow the (sulfidization) reaction on a given group of oxide nanoparticles.

Toward this goal, the time evolution of a group of nanoparticles was examined by sequential HREM viewing/reaction procedure. Figure 1A shows an assortment of molybdenum oxide particles which were sufidized in the GPR for 5 min.[13] The nanoparticles are made of a MoO_2 core covered by five or six closed layers of MoS_2. Subsequently, the grid was placed again in the reaction chamber and withdrawn after an additional 10-min reaction. Figure 1B shows the HREM image of the same group of nanoparticles. Clearly, an additional number of internal sulfide layers were formed at the expense of the encapsulated oxide and a hollow core is left in the center of each nanoparticle. These results give direct evidence in support of the growth mechanism of the inorganic fullerene-like nanoparticles from an oxide precursor as proposed before.[1]

3b. Influence of Hydrogen on IF Formation (Hydrogen-Free Reduction). According to thermodynamic calculations,[2,30] a reducing atmosphere is not required for the sulfidization of molybdenum or tungsten oxides. To test this point, WS_2 synthesis in hydrogen-free atmosphere was carried out. WO_3 powder with an average particle size of 150 nm was placed in the reactor (820 °C). Sulfur pressure (1 Torr) was provided by

(28) Homyonfer, M.; Mastai, Y.; Hershfinkel, M.; Volterra, V.; Hutchison, J. L.; and Tenne, R. *J. Am. Chem. Soc*. **1996**, *118*, 7804.

(29) Sanders, J. V. *J. Electron Microsc. Tech*. **1986**, *3*, 67.

(30) Knacke, O.; Kubaschewski, O. *Thermochemical Properties of Inorganic Substances*; Springer-Verlag, Berlin, 1991.

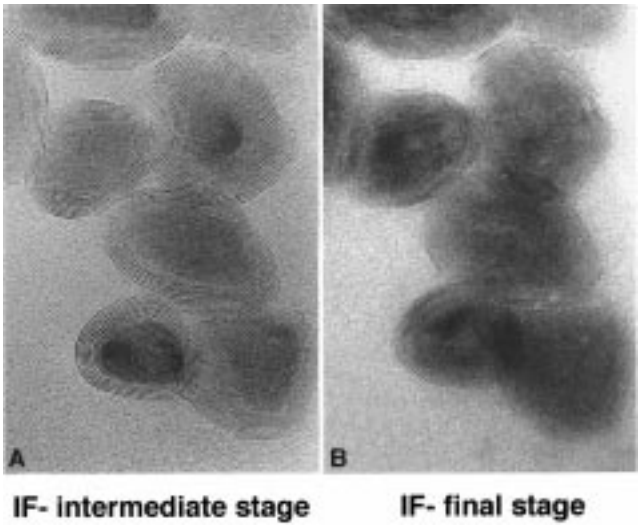

Figure 1. TEM images of a group of molybdenum oxide/molybdenum sulfide nanoparticles: (A) after 5 min anneal in H_2S/forming gas atmosphere; (B) after additional 10 min anneal in the same atmosphere.

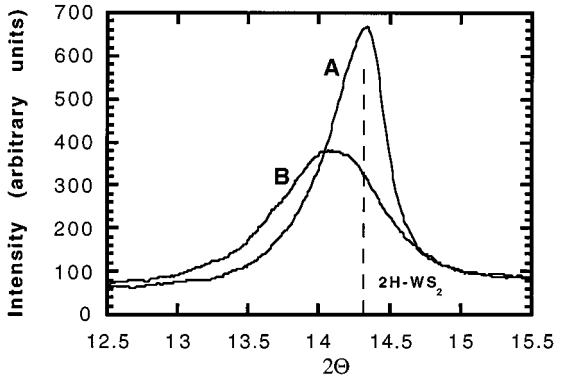

Figure 2. X-ray diffractograms of tungsten oxide converted into tungsten disulfide in the absence (curve A) and presence (curve B) of H_2.

preheating sulfur powder at 180 °C. The gaseous sulfur was transported to the reactor by the carrier gas (N_2). An TEM/XRD study shows that 2H−WS_2 platelets were obtained almost exclusively under these conditions. Figure 2A shows XRD of the reaction product. The position of the (0002) peak is in accordance with the conclusions of the TEM observation. However, when forming gas (5% H_2/95% N_2) was used instead of pure N_2, IF−WS_2 (Figure 2B) was obtained under the same experimental conditions. Both the shift of the (0002) peak of the XRD spectra (Figure 2B) and the TEM observations support this conclusion.[13] Thus, the IF phase cannot be obtained from the oxide nanoparticles without hydrogen. To further understand the influence of the reduction process on IF formation, the kinetics of the oxide reduction by hydrogen were investigated.

3c. Kinetics of WO_3 Reduction by Hydrogen. It is well-known that the reduction kinetics of oxides depend on the specific surface area of the powder.[31] Therefore, three kinds of WO_3 powders (>99% pure) with different average particle sizes were used. The first two oxide powders with average particle sizes of 3−5 μm and 150 nm were commercially available products. The third precursor oxide with particle sizes <30 nm was obtained by ball milling the second powder for 2 days. The oxide particles were multicrystalline with clear grain boundaries separating the different crystallites.

(31) Sloczynski, J.; Bobinski, W. *J. Solid State Chem.* **1991**, *92*, 436.

Table 1. Kinetics of the Reduction of WO_3 Nanoparticles into Suboxides

gas atmosphere, flow rate (cm^3/min)	average size of starting oxide particles (μm)	temp (°C)	reaction time (h)	product of reaction (XRD)	average particle size (TEM) (μm)
H_2 (1%)/N_2, 100	∼0.1	630	1.5	WO_3	
		650	1.5	$W_{20}O_{58}$	
	∼0.02	500	1.5	WO_3	
		530	1.5	$W_{20}O_{58}$	not changed
		560	2	WO_3	
		570	1.5	$W_{20}O_{58}$	
		600	1	$W_{20}O_{58}$ + $W_{18}O_{49}$ + W	0.06−0.1
H_2 (5%)/N_2, 100	∼0.1	650	1.5	WO_2 + W	0.03−0.1
		770	0.2	$W_{18}O_{49}$	0.1−1
			0.03		0.03−0.3
		820	0.3	$W_{18}O_{49}$	1−2
		970	0.3	WO_2 + W	1−6
	3−5	630	1	WO_3	not changed
		650	1.5	WO_3 + WO_2	0.1−3
		750	0.2	$W_{20}O_{58}$	
		970	0.3	WO_2	1−6

The experiments were performed in the open (flow) system, which was previously used for the SGR synthesis of IF.[1,13] The composition of the forming gas used for most experiments was (5% H_2/95% N_2). This composition was found to be the most suitable for IF synthesis. For the sake of comparison, another composition of the forming gas (1% H_2/99% N_2) was used in a few experiments. To cover the entire existence zone for IF formation, the temperature was varied over a wide interval (300−1000 °C). The reduction process of WO_3 goes through several intermediate stages. Initially a few suboxides phases are formed, followed by dioxide. Eventually the pure metal is obtained. The different intermediate phases can be observed by careful variation of the experimental parameters. With everything kept constant, all the intermediate phases of the reduction process could be followed by simply varying the annealing time of the experiment. The various crystalline phases were deduced from XRD measurements. The average particle size was estimated from the TEM images. Furthermore, TEM observations clearly demonstrated that each oxide particle consisted of smaller crystallites which were joined through their grain boundaries. Representative samples were taken for TEM examination during the reduction process. The results of these experiments are summarized in Table 1.

On the basis of the results presented in Table 1, the following inferences can be made:

1. The lower the concentration of hydrogen in the forming gas mixture, the slower was the reduction process and the higher was the temperature necessary for the reaction.

2. The size of the oxide particles plays an important role in the reduction process. The smaller are the oxide particles, the lower the temperature required to begin the reduction process.

3. The integrity of the oxide particles is preserved so that their initial shape is unchanged until some temperature is reached (∼600 °C). This temperature depends on the size of the starting oxide particles and the hydrogen concentration. Using TEM it was found that the grain boundaries between the crystallites

Table 2. Kinetics of the Reduction/Sulfidization of WO_3 Nanoparticles into Suboxides and Its Conversion into IF−WS_2

gas atmosphere, flow rate (cm^3/min)	average size of starting oxide particles (μm)	temp (°C)	reaction time (h)	product of reaction (XRD)	average particle size (TEM) (μm)
$S_2 + N_2$ subl., 100	∼0.1	840	1.5	2H−WS_2	<0.5
$S_2 + H_2$ (5%)/N_2 subl., 100				IF-WS_2	not changed
		650	0.5	IF-WS_2/$W_{20}O_{58}$	
	∼0.02	750	0.5	2H−WS_2 + $W_{18}O_{49}$	<0.5
		150	18	WO_3	
		300	9	WS_2/WO_3	
		400	4	WS_2/$W_{20}O_{58}$	
		500	18	PN−WS_2[a]	not changed
		700	0.3	IF-WS_2/$W_{20}O_{58}$	
	∼0.1	820	0.3	IF-WS_2/$W_{18}O_{49}$	
H_2S		820	2	IF-WS_2	
4.5		870	2	IF-WS_2 + 2H−WS_2 + $W_{18}O_{49}$	
H_2 (5%)/N_2, 100		970	1	2H−WS_2 + $W_{18}O_{49}$ + WO_2	2−10
		500	3	WO_3	not changed
		560	3	WS_2 + $W_{20}O_{58}$	
		620	1	WS_2 + $W_{20}O_{58}$	
	3−5	820	1	WS_2 + $W_{20}O_{58}$ + $W_{18}O_{49}$	0.1−3
		870	2	2H−WS_2 + $W_{18}O_{49}$	
		970	1	2H−WS_2 + WO_2 + $W_{18}O_{49}$	2−10

[a] PN = polycrystal nanoparticle.

disjoin and therefore the oxide particles tend to disintegrate into smaller particles. This process is believed to be facilitated by the crystallographic shear process (vide infra) occurring within the crystallites. The size of the shattered particles decreases with increasing temperature. XRD measurements did not discern changes in the (average) crystallites' size during the reduction process.

4. The two most abundant intermediate phases are $W_{20}O_{58}$ ($WO_{2.9}$) and $W_{18}O_{49}$ ($WO_{2.72}$). The first one is stable at lower temperatures, while the second phase is more typical of higher temperatures.

5. At elevated temperatures (above 700 °C), a secondary process of recrystallization of the oxide nanoparticles takes place. The recrystallized particles (typically >0.5 μm) are almost monocrystalline platelets even though the starting material consisted of polycrystalline oxide particles. In contrast to the shattered particles, the size of the recrystallized oxide particles increases with temperature.

6. Thus, one can distinguish between three temperature regions in which a different reduction behavior of trioxide particles is observed. Up to 600 °C the oxide particles do not change their initial shape during reduction; they break into smaller nanoparticles (less than 0.1 μm) at intermediate temperatures (600−700 °C) and grow to large platelets (more than 1 μm) at high temperatures.

3d. Kinetics of WO_3 Reduction/Sulfidization Combined. All the experiments of this series were performed in the same apparatus and using the same WO_3 powder as in the previous section. The addition of H_2S in the reaction chamber was the sole change. The data of this study are summarized in Table 2. As was reported in the previous work (ref 1), the sulfidization process of the oxide nanoparticles can be divided into two time domains. In the first stage, which lasts only a few seconds, the surface of the oxide nanoparticle is converted into a sulfide shell consisting of one or two monolayers of metal disulfide. In the second stage lasts 30−120 min or more.

The following inferences can be drawn on the basis of the results presented in Table 2:

1. Comparison between the results of Tables 1 and 2 shows that H_2S serves as an auxiliary reducer of the oxide.

2. At low temperatures, the rate of oxide sulfidization is higher than the reduction rate. For example, tungsten sulfide is obtained on the surface of the oxide particles (0.1 μm) after 9 h of annealing in forming gas + H_2S atmosphere already at 300 °C, while no reduction occurs under similar conditions for the same oxide particles.

3. The rate of reduction of the oxide particles increases with temperature much faster than the rate of sulfidization of the crystallites.

4. At elevated temperatures (>900 °C), large 2H−WS_2 crystallites are obtained by the reduction/sulfidization reaction from oxide particles of any size (0.1 μm to >3 μm).

5. Most surprisingly, while in the absence of H_2S gas (Table 1) both small and large particles breakdown into smaller particles, at temperatures between 600 and 850 °C, only the large particles disintegrate in H_2S atmosphere while small particles maintain their integrity.

6. There is a wide temperature interval (650−850 °C) in which the sulfide layer wraps an oxide nanoparticle (<200 nm), i.e., IF nanoparticle with oxide core is obtained. In this range of experimental parameters, the oxide core is progressively consumed and is converted into a hollow IF after 60−120 min.

7. Typically, large IF nanoparticles (100−150 nm) are produced from the corresponding oxide nanoparticles at 780−830 °C, while appreciably lower temperatures (600−700 °C) are required to obtain IF from the smaller oxide nanoparticles (10−30 nm).

8. During the conversion of oxide nanoparticles into IF−WS_2, the $W_{20}O_{58}$ ($WO_{2.9}$) phase is observed at 700 °C, while $W_{18}O_{49}$ ($WO_{2.72}$) is found to be the stable phase at 820 °C. As was noted above, MoO_3 is transformed into MoO_2 during IF−MoS_2 formation at 800 °C.

In view of the air sensitivity of sulfide particles, a series of experiments was conducted to check the time invariance of the sulfide/oxide composite nanoparticles. It was found that the XRD of a few samples which were analyzed in various time laps after they have been prepared did not show any time variation. This result is not surprising in view of the fact that the sulfide shell of nanoparticles is essentially seamless and the

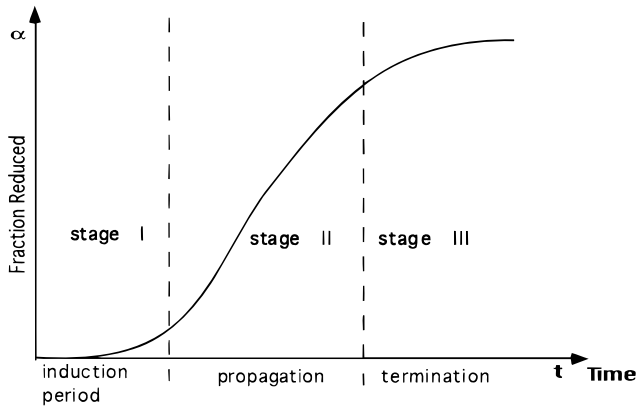

Figure 3. Schematic drawing describing the time evolution of the fraction of reduced oxide (α) for the nucleation model.

oxide core is protected from the ambient atmosphere by the sulfide shell.

4. Discussion

4a. MO_3 (M = Mo, W) Reduction Kinetics. In the majority of papers[34−40] dedicated to the reduction of MoO_3 by hydrogen or by hydrocarbons at temperatures below 600 °C, the degree of reduction, i.e., the ratio α of the reduced phase/total oxide, with time (*t*) was shown to exhibit a sigmoidal curve, which indicates that the rate of reaction versus $t - \alpha' = d\alpha/dt$ goes through a maximum (Figure 3). A similar characteristics for the reduction process of WO_3 has been documented.[41]

Figure 3 shows a schematic representation of the fraction of reduced oxide with respect to time α(*t*) for the nucleation model.[40] According to this model, the first stage of the reduction process is typified by an induction period during which oxygen vacancies accumulate at the oxide surface until a critical value is reached. If the critical value is high and the induction period is long, the first stage is a rate-limiting step for the entire process.

Presumably, an autocatalysis of the reduction occurs in the second stage (Figure 3). Since dissociative adsorption of hydrogen might be enhanced by the presence of reduced metal oxide, which has a higher density of coordinately unsaturated metal cations of lower oxidation states, the reduction process could be autocatalytic (propagation stage II). Therefore, the nuclei of reduced oxide, which are formed on the oxide particle surface, self-activate the reduction process. Moreover, as the grain size of the reduced oxide increases, the interfacial area between the reduced oxide grain and the oxide core expands and the supply of hydrogen increases, thereby increasing the rate of reduction as the process proceeds. Thus the fraction of reduced oxide as a function of time is concave upward (stage II in Figure 3) initially. Eventually, when the grains of reduced oxide coalesce in the oxide particle, the rate of reduction decreases with time (termination stage III). This explains the sigmoidal shape of the reduction curve.

Initially, the reduction of molybdenum trioxide to MoO_2 was considered to be a one-step reaction. Burch[37] was the first to recognize that Mo_4O_{11} is an intermediate product of the reaction. This hypothesis was confirmed experimentally by Ueno et al.,[39] who measured the rate of formation and disappearance of Mo_4O_{11} in the course of reduction of MoO_3 in a high-temperature X-ray chamber. Sloczynski,[42] analyzing the data of Ueno et al., has concluded that changes in the content of the intermediate and final product of the MoO_3 reduction can be ascribed to an autocatalytic effect. Note also that the intermediate MoO_{3-x} phases are substantially less stable than the intermediate phases of tungsten, i.e., $W_{20}O_{58}$ and $W_{18}O_{49}$. In the range of temperatures used in the present study, MoO_2 is the prevalent phase obtained upon reduction of MoO_3.

According to the nucleation model, surface oxygen atoms are removed from the lattice by reduction, leaving behind an anion vacancy.[43] When the concentration of vacancies reaches a critical value, the vacancies are annihilated by rearrangement of the lattice with the eventual formation of small grains of lower-valency oxide. Such rearrangement can be readily accomplished if the oxide particle tolerates the presence of crystallographic shear (CS) planes. The incipient oxide grains (on the surface of the oxide particle) grow inward by rearrangements of the reduced metal ions and diffusion of the oxygen ions outward. The shear process is more facile in the case of molybdenum oxide layered structure than for tungsten oxide (distorted ReO_3 structure), which explains the difference in the reduction kinetics of both phases (vide supra).

According to the calculations of Cormack et al.,[44] the concentration of vacancies in equilibrium with shear planes decreases with temperature. Therefore, lower critical concentration (threshold value) of vacancies is required for the shear process to occur at higher temperatures. On the other hand, the rate of vacancy formation increases with temperature. Therefore, the induction period for generation of threshold concentration of vacancies on the crystallite surface decreases with temperature. Indeed, experimental data show that at elevated temperatures (above 600 °C) the trioxide particles disintegrate and are broken into smaller suboxide crystallites within a few minutes. Apparently, the fast shear process causes disintegration of the oxide particles. Thus, the first step of reduction ($WO_3 \rightarrow WO_{3-x}$) at high temperatures cannot be described by the nucleation model and the shear process becomes a rate-limiting step.

The shear process (stage II) is equivalent to the hopping of an atom to neighboring vacancy in the lattice, however it is believed that the octahedron hops as a whole at the instant of the event (Figure 4C). The diffusion of a vacancy can be described as a sequence of jumps which are described by the Frenkel model.[45] According to this model, the hoping frequency, *p*, which is in fact the probability that sometime during a unit time the atom will have sufficient thermal energy to pass over the barrier between neighboring atoms, is

(32) Muijsers, J. C.; Weber, Th.; van Hardeveld, R. M.; Zandbergen, H. W.; Niemantsverdriet, J. W. *J. Catal.* **1995**, *157*, 698.
(33) Spevack, P. A.; McIntyre, N. S. *J. Phys. Chem.* **1993**, *97*, 11031.
(34) Batist, Ph. A.; Karteijns, C. J.; Lippens, B. C.; Shuit, G. C. A. *J. Catal.* **1967,** 7.
(35) Chijikov, D. M.; Ratner, Yu, E.; Tsvetkov, Yu, V. *Izv. Akad. Nauk SSR Metal.* **1970**, *70*, 8.
(36) Ratnasamy, P.; Ramaswamy, A. V.; Banerjee, K.; Sharma, D. K.; Ray, N. *J. Catal.* **1975**, *38*, 19.
(37) Burch, R. *J. Chem. Soc., Faraday Trans.* **1978**, *74* (12), 2982.
(38) Gajardo, P.; Grange, P.; Delmon, B. *J. Chem. Soc., Faraday Trans.* **1980**, *76*, 929.
(39) Ueno, A.; Kotera, Y.; Okuda, S.; Bennet, C. D. *Chem. Uses Molybdenum Proc. Int. Conf. 5th* **1982**, 250.
(40) Transition metal oxides: *Surface Chemistry and Catalysis*, Kung, H. H., Ed.; Amsterdam, Oxford, New York, Tokyo, 1989.
(41) Guo, J.-D.; Whittingham, M. S. *Int. J. Modern Phys. B* **1993**, *7*, 4145.
(42) Sloczynski, J. *React. Solids* **1989**, *7*, 83.
(43) Miyano, T.; Iwanishi, M.; Kaito, C.; Shiojiri, M. *Jpn. J. Appl. Phys.* **1983**, *22* (5), 863.
(44) Cormack, A. N.; Jones, R. M.; Tasker, P. W.; Catlow, C. R. A. *J. Solid State Chem.* **1982**, *44*, 174.
(45) *Introduction to solid-state physics*, 6th ed.; Kittel, Ch. Ed.; Brisbane, Toronto, Singapore, 1986; p 520.

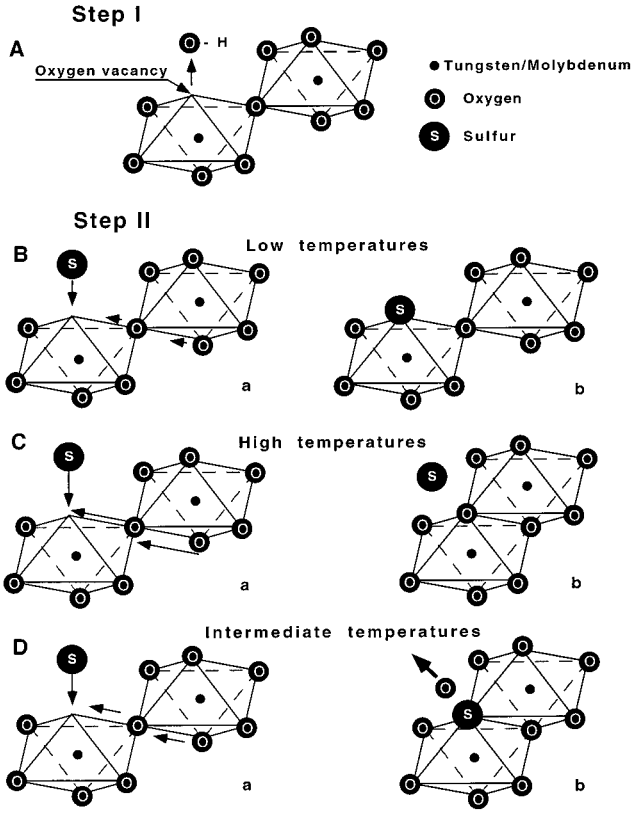

Figure 4. Schematic drawing of the various processes which occur during the sulfidization of the metal oxide particles. The oxide precursor is represented as two octahedra connected via a corner oxygen atom. (A) Preliminary step: oxygen atom leaves the octahedron, and oxygen vacancy is thus formed. The three possible subsequent steps are shown below: (B) Sulfidization of the oxide at low temperatures. The rates of the processes are represented schematically through the size of the arrows. Thus, the rate of the shear process is slow compared with sulfur trapping by the vacancy and consequently sulfur trapping predominates. (C) Sulfidization of the oxide at high temperatures. The rates of both the shear process and sulfur trapping increase with temperature; the former one predominates however. Therefore, shear (reduction of the oxide) prevails at these temperatures. (D) At intermediate temperatures (600−850 °C), the rates of both processes are on the same order of magnitude and the sulfidization and shear appear at the same time, leading to the formation of the superficial sulfide layer engulfing the oxide nanoparticle. Representation of the situation (a) prior to the process and (b) after the process has been completed.

$$p = \upsilon \exp(-E_b/k_B T) \qquad (1)$$

where E_b is the energy barrier height between neighboring atoms, k_B is the Boltzmann constant, and T is the absolute temperature. Since the octahedra form a kind of an extended network, the vibration frequency (υ) of the surface octahedra grows up as the size of the oxide particle decreases (Figure 5A). The relaxation time of vacancy annihilation by the shear mechanism is equal to $1/p$ and decreases exponentially with temperature.

In a number of papers,[33,46] including the present one, the presence of sulfur in the reaction chamber was found to catalyze the reduction process. Apparently, oxygen−sulfur exchange influences the autocatalytic reduction mechanism. Indeed, when sulfur replaces oxygen in the corner of an octahedron, the degree of unsaturation of the metal cation increases, since sulfur is less electronegative compared with oxygen. Furthermore, the higher degree of unsaturation of the metal cation increases the dissociative adsorption of hydrogen. Therefore, the addition of sulfur accelerates the rate of the reduction process.

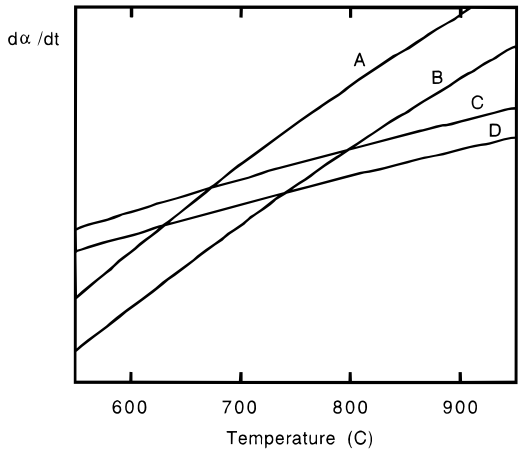

Figure 5. Calculated rate of reduction of small (A) and large (B) oxide nanoparticles and sulfidization (C) and selenization (D) as a function of temperature.

4b. MO_3 Reduction/Sulfidization Kinetics. The mechanism of the reaction $MO_3 \rightarrow MS_2$ is still under debate.[32,33,46,47] Although MO_3 sulfidization occurs more readily in H_2/H_2S mixtures than in pure, dry sulfur, the role of hydrogen in the sulfidization process can be different depending on the reaction temperature.

Temperature-programmed sulfidization was used[32,47] for studying the sulfidization of MoO_3 thin films on SiO_2 support. Analysis of the Mo 3d and S 2p lines of the XPS spectra suggested that two temperature regimes could be recounted for this reaction. At low temperatures and up to 600 °C, the first step is an oxygen/sulfur exchange at the surface of the oxide precursor without reduction of the metal atoms. This exchange, which takes place already at room temperature, results in S^{2-} ligands bonded to Mo^{VI} centers (Figure 4B). In the next stage of the sulfidization process, reductive elimination of S atom from the bridging S_2^{2-} ligands accompanied by the formation of Mo−S−Mo bonds and the release of H_2S takes place.[32] At high temperatures reduction of the metal atoms prevails (vide infra).

Spevack and McIntyre[33] also established that O−S exchange occurred on Mo^{VI} atoms at low temperatures. They further speculated that much higher energies would be required for sulfur to break the multiple Mo−Mo bonds in MoO_2.[33] Indeed, Grange[46] and the present study have both indicated that the formation of MoO_2 hinders (slows down) the sulfidization even at high temperatures.

As noted above, the sulfidization rate prevails over the reduction step at low temperatures and the reactivity of hydrogen as reductant of MO_3 increases with temperature. Since the rate of reduction at elevated temperatures (up to 1000 °C) is very fast, the sulfidization of the oxides takes place after the reduction of MoO_3 to MoO_2 has been completed.[47] Sulfidizing in this range of temperatures can be therefore described mainly as O−S exchange bound to Mo^{IV} atoms.[47] The present study shows that at high temperatures (>600 °C) WO_3 reduces very quickly to suboxide phase WO_{3-x} and subsequently it is slowly transformed into the respective sulfide (see Table 2).

Therefore, the relationship between reduction and sulfidization rates determines the kinetics of reduction/sulfidization of the oxide. At low temperatures, the induction period of the

(46) Grange, P. *Catal. Rev.-Sci. Eng.* **1980**, *21* (1), 135.

(47) Arnoldi, P.; van den Heijkant, J. A. M.; de Bok, G. D.; Moulijn, J. A. *J. Catal.* **1985**, *92*, 35.

reduction is rather long and the sulfidization is accomplished before the reduction of the nanoparticles has started. At high temperatures, the first step of reduction from trioxide to suboxide is very quick and the sulfidization takes place only after reduction of the oxide nanoparticles. This situation further slows the rate of sulfur/oxide exchange, since much higher energies would be required for sulfur to break the stronger oxygen−metal bond of sub- or dioxide as compared with this bond in trioxide. The transition zone between the two regimes is discussed separately below.

The creation of oxygen vacancies on the surface of the oxide particles, by hydrogen, is most probably the first step in the entire (reduction−sulfidization) process (Figure 4A). Thence two competing events follow: the first one is vacancy annihilation by the shear process; the second event is sulfur occupation of the oxygen vacancy site. As noted above, sulfur occupation of the vacancy sites is more rapid than vacancy annihilation by a shear process at low temperatures (Figure 4B), while the reduction process prevails at high temperatures (Figure 4C).

The exponential dependence of the relaxation time of the shear process on temperature was discussed above. The relaxation time of the oxygen vacancy on the crystallite surface through sulfur occupation can be estimated from the kinetic theory of gases. The sulfur concentration defines an average distance between a vacancy on the particle surface and the nearest sulfur atom in the gas atmosphere. The kinetic energy of a particle in the gas atmosphere is equal to k_BT, and hence, the average velocity (V) of a sulfur atom is

$$V = (2k_BT/m)^{1/2} \quad (2)$$

where m is the mass of a sulfur atom. Thus, for a certain sulfur concentration, the relaxation time of oxygen vacancy by sulfur occupation is inversely proportional to the square root of the temperature.

4c. Synergistic Model. Figure 5 illustrates the schematic rates of reduction (A and B), sulfidization (C), and selenization (D) as a function of temperature. To plot this graphs, the functional dependence of the shear (eq 1) and sulfidization (eq 2) on temperature were calculated using arbitrary parameters, so that a single cross point between the two rates was obtained. Therefore the plots have qualitative significance only and they do not intend to represent a detailed calculation of the kinetic process. The sulfidization (selenization) reaction goes faster at low temperatures. Conversely, the reduction rate is much larger at high temperatures. The cross point of the reduction and sulfidization (selenization) curves shows the temperature range where the reduction rate is equal to the sulfidization (selenization) rate. It is suggested that instead of a competition between the two processes, a *synergy of the two processes exists* at this range of temperatures.

Figure 4 shows a schematic drawing of the shear (reduction) and sulfidization processes at different temperatures. The first step (step I) of vacancy formation by abstraction of one oxygen atom by a hydrogen atom is common to all temperatures. In the next step (II), any of three processes can take place; their relative rates vary with the temperature. At low temperatures, sulfur trapping is relatively faster than shear (Figure 4B). Conversely, at high temperatures, the shear process is faster (Figure 4C). At intermediate temperatures (600−850 °C), the rates of the two processes are equivalent (for a given experimental parameters this range is much narrower). During the shear of an octahedron, the oxygen atom, which hops from one corner to a neighboring vacancy, has to break its chemical bond to its nearest metal neighbor, and consequently, it is more prone to a chemical reaction or substitution at this instant of time. When the probability of oxygen leaving (reduction of oxide) equals the probability of the sulfur occupation of the oxygen vacancy site, the kinetic rate of the oxygen substitution by sulfur is the largest (Figure 4D). On the other hand, as noted above, the sulfur−oxygen exchange accelerates the autocatalytic reduction effect. Thus, a synergy between the autocatalytic reduction and oxygen−sulfur exchange prevails when the rates of the two processes are equivalent.

From the microscopic viewpoint, there is a significant difference between the low (high)-temperature processes and those at intermediate temperatures. In the low and high-temperature processes (Figure 4B,C), no oxygen atom is abstracted. In contrast to that, one oxygen atom is released when the synergy between the two processes (shear/sulfidization) occurs (Figure 4D). Moreover, this situation leads to the bonding of the captured sulfur atom to two neighboring M^V atoms, which is opposite to the situation at low temperatures. Subsequent abstraction of oxygen atoms and shear and concomitant sulfur atom capturing from the gas phase promotes the growth of the MS_2 surface layer encasing the oxide nanoparticle.

As shown above (section 3b), in the absence of hydrogen, sulfidization of the oxide leads to the formation of 2H−WS_2. It is believed that the *synergy between the reduction and sulfidization processes provides the conditions for IF formation in a certain range of experimental parameters*. Following the formation of sulfide nuclei on the surface of an oxide nanoparticle, these two processes proceed simultaneously. The reduction process extends quickly inward by the fast rearrangements of the lattice and the formation of shear planes. This process leads to the "recrystallization" of the suboxide nanocrystal. On the other hand, oxygen/sulfur exchange cannot extend inward (into the particle core) due to steric hindrance of sulfur diffusion into the oxide core. The fast-growing sulfide layer replicates the morphology of the surface of the oxide nanoparticle. The anisotropy of the sulfide growth rate provides no time for a 3-D growth pattern of the nanocrystal and, thus, further promotes the formation of the curved sulfide 2-D (001) layer. It should be noted that the growth rate of the sulfide layer on the surface of the large oxide particles is not sufficient to wrap the entire surface, while reduction of the oxide takes place and they all break up into smaller crystallites (Table 2), which precludes IF formation from large oxide particles.

The formation of a *thin sulfide skin controls the size of the fullerene-like nanoparticle*. Once the size and shape are fixed, further transformation of the oxide into sulfide takes place internally. The growth of the next inner sulfide layers does not change the morphology of the outer layers (Figure 1). Therefore, sulfur and oxygen diffuse through available faults in the sulfide shell.[1]

The quasi-spiral inward growth process of the curved sulfide layers predetermines the hollow core of the fullerene-like nanoparticle. Every inner sulfide layer grows under a neighboring outer one. The radius of curvature of the innermost layers decreases as the process proceeds. The smallest radius of curvature of the sulfide layer, which corresponds to the minimum hollow core size, was found to be 1.4 nm.[13] However, most IFs have larger hollow cores.[13] The oxide core engulfed by the first closed sulfide shell is the precursor for the subsequent sulfide growth. The density of the crystalline metal oxide is higher than that of the metal sulfide. The presence of a hollow core in the IF particle suggests that the density of the primary oxide nanoparticles is much less than the formal density

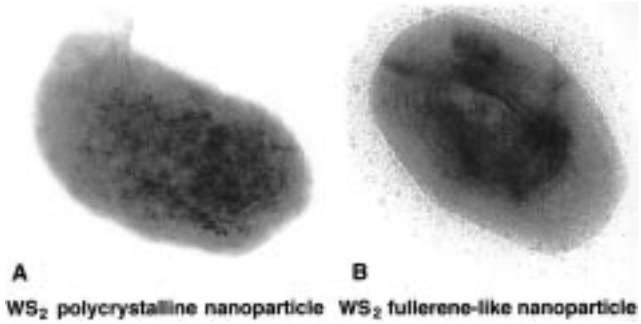

Figure 6. TEM images of polycrystalline (A) and onion-like (B) tungsten sulfide nanoparticles.

of the (monocrystal) oxide. Moreover, it is sometimes observed that the volume of the first shell of the sulfide layer (skin) can be appreciably larger than the volume of the starting oxide nanoparticle, leaving thus a free void between the sulfide skin and the oxide. Thus, the size of the hollow core of the IF is defined by the experimental conditions of this concrete nanoparticle.

As noted above,[1] the size of the precursor oxide particle defines the final dimensions of the IF particle. According to the synergy model (Figure 5), smaller oxide nanoparticles are wrapped by a sulfide layer at lower temperatures than bigger ones, which is confirmed by the experimental data (see Table 2). It is noticed that the size and shape of the IF particles follow closely those of the oxide precursor (see Figure 2 of ref 1).

Figure 6 shows TEM images of a polycrystalline (A) and fullerene-like (B) nanoparticles of WS_2. The polycrystalline nanoparticles were grown at 500 °C. This temperature is below the temperature corresponding to the *synergy effect*. The polycrystalline sulfide nanoparticle, like its oxide precursor nanoparticle, consists of very small randomly oriented nanocrystallites. Oppositely, the IF particle, which is formed via the *synergy effect* at much higher temperatures (800 °C), consists of a single domain and consequently has the long-range order of the curved atomic (metal disulfide) layers.

Synthesis of IF−WSe_2[2] shows also a good agreement with the present model. The cross point between the reduction and selenization processes (Figure 5) is observed at lower temperatures (typically 760 °C) compared with 840 °C for IF sulfide formation. Higher reaction temperatures yielded platelets (2H) of the respective selenides. Hence, the synergism between selenization and reduction, which is a prerequisite for the IF formation, occurs at lower temperatures than that of the respective sulfide. This tendency is confirmed by the available experimental data[2] and is further supported by preliminary data for IF of metal telluride's (630 °C). However, in this last case, it is unlikely that dislocation-free IF will be obtained at such low temperatures.

5. Conclusions

Direct evidence for the formation mechanism of the first fullerene-like layer of MX_2 (M = W, Mo; X = S, Se, Te) on the surface of oxide nanoparticle is demonstrated. This process is followed by a chalcogen/oxide exchange for which a direct proof is demonstrated on the same group of nanoparticles which were reacted step by step. It is shown that hydrogen is a necessary precursor for IF formation from metal oxide nanoparticles.

The synergy between the reaction of the chalcogen molecules coming from the gas phase and the reduction process of the oxide for IF−WX_2 (X = S, Se) synthesis is consistent with the available experimental data. Further work is necessary to provide a direct proof of this unique process.

Acknowledgment. We are grateful to Dr. J. Sloan of the University of Oxford for his useful suggestions regarding the SC process. This research was funded by the following grants: UK-Israel Science and Technology Foundation; NEDO (Japan) International research program; Israeli Ministry of Science (strategic research program on nanomaterials); Petroleum Research Foundation of the American Chemical Society; Minerva Foundation (Munich).

JA973205P